International Journal of Nanoelectronics and Materials
Volume 12, No. 4, Oct 2019 [495-516]

Defective TiO_2 with Intrinsic Point Defects for Photocatalytic Hydrogen Production: A Review

Sawsan Abdullah Abduljabbar Anaam[1], Hashim Saim[1*], Mohd Zainizan Sahdan[1] and Adel Al-Gheethi[2]

[1] *Microelectronics & Nanotechnology-Shamsuddin Research Centre, Universiti Tun Hussein Onn Malaysia, 86400 Parit Raja, Batu Pahat, Johor, Malaysia.*
[2] *Department of Water and Environmental Engineering, Faculty of Civil & Environmental Engineering, Universiti Tun Hussein Onn Malaysia, 86400 Parit Raja, Batu Pahat, Johor, Malaysia.*

Received 18 March 2019, Revised 30 May 2019, Accepted 26 June 2019

ABSTRACT

Titanium dioxide (TiO_2) has been intensively investigated for solar hydrogen conversion via photocatalytic and photoelectrochemical water splitting. However, the performance of TiO_2 photocatalyst for hydrogen generation is low due to the rapid electron-hole recombination and its wide band gap (3.0-3.2 eV) which is only feasible for UV light absorption of solar spectrum. There are various strategies have been used for TiO_2 modification to harvest the sunlight and improve the surface chemical reaction between TiO_2 and H_2O for water splitting. Among the TiO_2 modification strategies, intrinsic point defects such as vacancies and interstitials in TiO_2 have been proven to improve the TiO_2 properties for photo-catalytic activity. In this article, the recent progress achieved in defective TiO_2 with intrinsic point defects for photocatalytic hydrogen evolution and photoelectrochemical water splitting has been reviewed. The fabrication methods of defective TiO_2 along with their structural, optical, and charge carrier properties have been introduced. It has appeared that the intrinsic point defects are a promising strategy to improve the performance of TiO_2 for photocatalytic hydrogen production, and more efforts are still needed to improve the TiO_2 performance for photocatalytic hydrogen production in this area of research.

Keywords: TiO_2 Surface, Vacancies, Interstitials, Photoelectrochemical Water Splitting, Photocatalytic Hydrogen Evolution, Intrinsic Point Defects.

1. INTRODUCTION

Photocatalytic hydrogen production is being considered as a promising route for supplying environmentally friendly and sustainable energy. There are two methods to produce hydrogen directly from the sunlight: photocatalytic (PC) and photoelectrochemical (PEC) water splitting [1,2]. Semiconductor photocatalysts have been considered to be used for the conversion of solar energy to chemical energy. When the photocatalyst absorbs photons of sunlight with energy greater than or equal to its band gap, the electrons are excited from the valence band (VB) to the conduction band (CB) and then the photoinduced electron-hole pairs are formed. The holes oxidize the water to oxygen and the electrons reduce protons (H^+) to hydrogen, respectively [3]. However, most of semiconductors have ability to absorb UV light which constitute only 4% of solar spectrum. Therefore, in order to improve the solar hydrogen conversion, a modification of photocatalyst properties should be conducted to improve the visible light absorption, which constitute 43% of solar energy. Besides, low-cost and stable semiconductors are required [4,5].

*Corresponding Author: *hashim@uthm.edu.my*

Titanium dioxide (TiO_2) is one of the most attractive materials which is used as a photocatalyst for hydrogen production because it is a non-toxic, cheap, abundant and stable in aqueous solutions. Besides, it has the right conduction and valence band edge position for water reduction and oxidation. However, TiO_2 still has some limitations as a photocatalyst in terms of wide band gap 3.0 eV (415 nm) for rutile and 3.2 eV (380 nm) for anatase. Therefore, TiO_2 only absorbs light in the ultraviolet (UV) region. Moreover, the photogenerated charge carrier recombination of TiO_2 is high [4,6]. Thus, due to the low harvesting of sunlight and rapid recombination of charge carrier, TiO_2 is not efficient enough for hydrogen production. In order to overcome these limitations, various strategies have been used to improve the photocatalytic hydrogen production by water splitting. The metal or non-metal doping in TiO_2 has been extensively used to enhance the photocatalytic activity of TiO_2. However, the high concentration of dopants creates recombination center and the low concentration of dopants is not enough for the visible light absorption [7-10]. In addition, metal loading such as Ag or Au nanoparticles has been widely investigated for enhancement of the visible light absorption due to the surface plasmon resonance [11,12]. Moreover, the metal co-catalyst like Pt and Pd prevent the charge carrier recombination. However, all these metals are expensive to be used for enhancing the absorption of TiO_2 [13,14]. Furthermore, semiconductor heterojunction is a common method to modify the photocatalytic properties of TiO_2. In general, when p- and n-type semiconductors are in contact, the electrons and holes are diffuse and form a built-in electrical potential. The formation of the electrical field might enhance the charge separation and improve the photocatalytic activity of TiO_2 [15]. Nonetheless, the accumulation of electrons might create a photo-corrosion for one of semiconductors or both of them [16].

Apart of the above-mentioned strategies, intrinsic point defects have attractive attention to promote the photocatalytic properties of TiO_2 for hydrogen production. These defects have essential impact to improve TiO_2 performance for H_2 generation. For instance, oxygen vacancies/Ti^{3+} extend the light absorption to visible light and enhance the charge carrier separation [17,18], while titanium vacancies increase the charge mobility [19]. Furthermore, defective TiO_2 with oxygen vacancies/titanium vacancies increase the photocatalytic activity for hydrogen production [20].

This review focuses on the recent developments in intrinsic point defects in TiO_2 for photocatalytic hydrogen evolution and photoelectrochemical water splitting. In addition, the basic principles and preparation methods of intrinsic point defects in TiO_2 are discussed. The structural, optical and charge transfer properties are reviewed.

2. PRINCIPLES OF INTRINSIC POINT DEFECTS IN TiO_2

Intrinsic point defect of TiO_2 has been considered in terms of ionic and electronic defects. The ionic defects in TiO_2 include oxygen vacancies (V_o), titanium interstitials (Ti_{int}), titanium vacancies (V_{Ti}), and oxygen interstitials (O_{int}), while the electronic defects involve electrons and electron holes as shown in Figure 1(a). The electrons are located on Ti^{3+} ions in their lattice sites, whereas, the electron holes are located on lattice sites of O^- ions. These defects occur due to the introduction of disorder in the crystal pattern of TiO_2 [21-24]. Oxygen vacancies and titanium interstitials are donors of electrons and form donor level in the electronic structure of TiO_2. The existence of the donors shifts the Fermi level towards the lower part of the band gap. In contrast, the titanium vacancies and oxygen interstitials are acceptors and form acceptor level in TiO_2. As a result, the presence of the acceptors moves the Fermi level towards the upper part of the band gap. For instance, the oxygen vacancies and titanium vacancies form energy levels in TiO_2 at 1.18 and 1.15 eV, respectively [23-28].

Additionally, defects enhance the photocatalytic activity of TiO_2. For instance, titanium vacancies act as surface active sites for adsorption of water on TiO_2 surface. Titanium vacancies are needed to transfer electrons from water molecules to TiO_2 surface in order to enhance the oxidation reaction [29]. As depicted in Figure 1(b), when the water molecules are adsorbed on the specific surface-active site (titanium vacancies), the titanium vacancies have a strong electron affinity and the ability to donate electron holes. Active complexes of titanium vacancies are formed when electrons holes transfer to adsorbed water species. These active complexes are metastable and decomposed into gaseous oxygen and hydrogen ions [26].

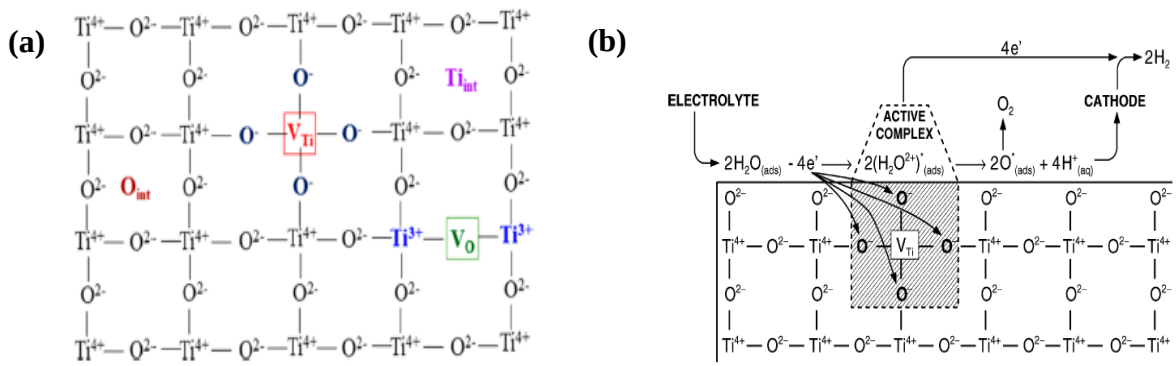

Figure 1. (a) Intrinsic point defects in TiO_2 [19]. (b) titanium vacancies(V_{Ti}) in TiO_2 for charge transfer and water decomposition [26].

3. PREPARATION METHODS FOR INTRINSIC POINT DEFECTS IN TiO_2

Several strategies were employed to form the intrinsic point defects in TiO_2 as summarized in table 1. Ti^{3+}/oxygen vacancy defects could be fabricated using various metheds such as hydrogenation, and reduction. The thermal treatment with hydrogen gas (hydrogenation) was reported to form Ti^{3+}/oxygen vacancies. Amano *et al.* [30] calcined TiO_2 (anatase phase/rutile phase = 3.4/ 96.6 wt %) under hydrogen gas. TiO_2 was treated in calcination temperature range of 300−1100 °C under hydrogen gas flow rate of 50 mL/ min at atmospheric pressure, and then the samples were cooled down to room temperature. Hydrogen treatment at calcination temperature 500 °C formed Ti^{3+}, whereas the density of electrons was enhanced at 700 °C. Liu *et al.* [31] fabricated the Ti^{3+}/oxygen vacancies in TiO_2 using a high pressure H_2 treatment. The Ti^{3+} formation was recorded at 500 °C under hydrogen pressure 20 bar. The oxidation of TiH_2 in H_2O_2 was also reportd to form Ti^{3+} in TiO_2. Liu *et al.* [32] Synthesized Ti^{3+} self-doped anatase TiO_2 by oxidation of TiH_2 in H_2O_2 which followed by the calcination temperature (300-600 °C), calcination time (2-4 h) and flow rate of argon was at 20 mL min^{-1}. Ti^{3+} self-doped TiO_2 nanoparticles in a pure anatase phase were formed at 500◦C for 4 h. Grabstanowicz *et al.* [33] also used the oxidation of TiH_2 in H_2O_2 to form Ti^{3+}/TiO_2 in rutile phase as directed in Figure 2(a), the gray TiH_2 reacted with H_2O_2 and formed yellow gel which calcined at 630 °C for 3 h under argon flow to form black Ti^{3+}/TiO_2 powder. Wei *et al.* [34] synthesized Ti^{3+} self-doped anatase TiO_2 by using H_2O_2 with hydrothermal method. It was observed that when the hydrothermal reaction time was 12 h and the amount of H_2O_2 was 100 µL, oxygen vacancies were formed after calcination with N_2.

Table 1 Synthesis, properties and applications of defective TiO_2 with intrinsic point defects.

Fabrication method	Phase	Morphology	Defect	Application	Reference
Hydrogenation of TiO_2	Pure rutile or anatase-rutile mixed phase	particles and films	Ti^{3+} ions/ oxygen vacancies	Water oxidation	[30]
Hydrogenation of TiO_2 with high pressure	Anatase	Nanotubes	Ti^{3+} ions/ oxygen vacancies	Photocatalytic hydrogen production	[31]
Oxidation of TiH_2 in H_2O_2	Anatase	Nanoparticles	Ti^{3+} ions/ oxygen vacancies	Photodegradation of Methylene blue (MB)	[32]
Oxidation of TiH_2 in H_2O_2	Rutile	Nanoparticles	Ti^{3+} ions	Photodegradation of organic species in water	[33]
Hydrothermal method	Anatase	Nanorod-type microstructure	Ti^{3+} ions/ oxygen vacancies	Photocatalytic hydrogen production	[34]
Reduction with $NaBH_4$	Anatase	Nanoparticles	Ti^{3+} ions/ oxygen vacancies	Photodegradation of methyl orange and phenol	[38]
Reduction with $NaBH_4$	Anatase-rutile mixed phase	Nanoparticles and hierarchical structures	Ti^{3+} ions/ oxygen vacancies	Photodegradation rate of methylene blue	[39]
Reduction with $NaBH_4$	Anatase	Nanobelts	Ti^{3+} ions/ oxygen vacancies	Photodegradation of methyl orange and water splitting for hydrogen production	[40]
Reduction with $NaBH_4$	Anatase	Nanotube arrays	Ti^{3+} ions/ oxygen vacancies	Photoelectrochemical water splitting	[41]
Reduction with $NaBH_4$	Anatase	Nanoparticles	Ti^{3+} ions/ oxygen vacancies	Rhodamine B photodegradation	[42]
Solvothermal method	Anatase	NM	Titanium vacancies	Photodegradation of organic pollutants and photocatalytic hydrogen production	[19]
Thermal oxidation	Rutile	NM	Titanium vacancies	NM	[49, 50]
Sol–gel method	Anatase	Thin film	P-type TiO_2	Acetone detection	[51]
Atomic layer deposition	Rutile	Thin film	Oxygen interstitials	As homojunction diode	[43]
Decorating n-type TiO_2 QDs on p-type TiO_2 sheets	Anatase	Particles	P-n homojunction(oxygen/ titanium vacancies)	Photoelectrochemical and photocatalytic hydrogen generation	[20]
Sol gel method with UV light pre-treatment	Anatase	Nanoparticles	Titanium vacancies titanium interstitials	Photocatalytic hydrogen production	[24]

NM: Not Mentioned.

The reduction method has also been utilized for intrinsic point defects formation in TiO_2. The utilization of $NaBH_4$ to form oxygen vacancies/Ti^{3+} in TiO_2 have been reported by many authors in the literature[35-42]. Xing *et al.* [38] used Solvo-thermal method with $NaBH_4$ for Ti^{3+}/oxygen vacancies formation in TiO_2. After adding 0.13 g of $NaBH_4$ as reduction agent, Ti^{3+}/oxygen vacancies were formed. In another study, TiO_2 powder with different amount of $NaBH_4$ was used to form Vo/Ti^{3+} by hydrothermal method. Addition of 12 g of $NaBH_4$ to TiO_2 exhibited the highest photocatalytic degradation efficiency of methylene blue [39]. Tian *et al.* [40] synthesized TiO_2 nanobelts with Vo/Ti^{3+} by using $NaBH_4$ with heat treatment and argon gas. The defects were

formed by adding of 5 mL of $NaBH_4$, and heat treatment at 380 °C for 24 h. It was claimed that $NaBH_4$ reduced Ti^{4+} to Ti^{3+} as is shown in the following reaction (1) and (2).

$$NaBH_4 + 8OH^- \rightarrow NaBO_2 + 8e^- + 6H_2O \quad (1)$$
$$Ti^{4+} + e^- \rightarrow Ti^{3+} \quad (2)$$

Kang *et al.* [41] used $NaBH_4$ as a reduction agent to form oxygen vacancies on the surface and interior of the TiO_2 nanotube arrays (NTAs). NTAs were fabricated by anodizing a Ti foil in ethylene glycol solution including NH_4F (0.3 wt%) and H_2O (2 vol%) at 80 V for 30 min with a graphite cathode. The nanotube arrays were annealed at 450°C for 3 h. To form the oxygen vacancies, NTAs were dipped in $NaBH_4$ at room temperature for different times. Ariyanti *et al.* [42] synthesized defective TiO_2 with oxygen vacancies. TiO_2 nanoparticles were mixed with $NaBH_4$ and then heated at temperature in the range 300-450 °C with Ar. The color of TiO_2 has changed when the treatment temperature was changed as shown in Figure 2(b).

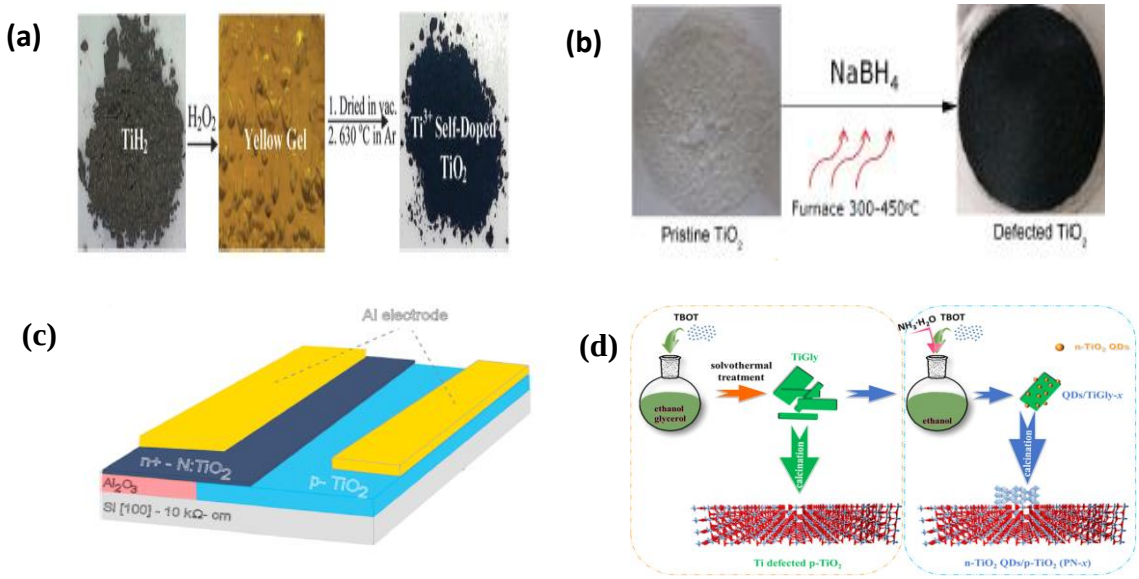

Figure 2. Schematic diagram of : (a) synthesis of Ti^{3+} self-doped rutile TiO_2 using oxidation process [33]. (b) synthesis of Ti^{3+} self-doped TiO_2 using reduction agent[42]. (c) synthesis of p-type TiO_2 using atomic layer deposition[43]. (d) formatiom of TiO_2 p-n homo-junction using in-situ decorating n-type TiO_2 QDs on p-type TiO_2 sheets[20].

In addition, there are other methods which have been used to form the intrinsic defects. Blue Ti^{3+} self-doped anatase-rutile mixed phase TiO_2 nanoparticles were fabricated by solvothermal method [44]. Sasikala *et al*. [45] synthesized Ti^{3+} nanoparticles by various methods which were solvothermal, sonochemical and polyol methods. Saputera *et al.* [46] used three different methods to synthesize TiO_2 with Ti^{3+} and oxygen vacancies defects. Reduction, calcination, and hydrogenation methods were used to fabricate the nanoparticles with the defects. Ice-water Quenching and Imidazole(as reducing agent) also were utilized for preparation of intrinsic defects [47,48].

In comparison to Ti^{3+} self-doped TiO_2, few studies have been conducted for the formation of un-doped p-type TiO_2 with titanium vacancies or oxygen interstitials. Wang *et al*. [19] formed TiO_2 with titanium vacancies by solvothermal treatment of tetrabutyl titanate in an ethanol–glycerol mixture and then the product was calcined at 470 °C for 1 h. In another study, V_{Ti} was formed in rutile TiO_2 by thermal oxidation at temperature 1323 K for ~ 3450-3500 h and under oxygen pressure = 75 kPa [49,50]. Bhowmik *et al*. [51] synthesized undoped anatase p-type TiO_2 by sol–gel method, and then it was deposited on thermally oxidized p-type Si substrate by drop coating.

After that the product was annealed in air at 450 °C for 3 h. However, it was not explained if the p-type properties of TiO_2 either due to titanium vacancies or oxygen interstitials existence. Iancu *et al*. [43] synthesized undoped p-type TiO_2 films with oxygen interstitial defects by atomic layer deposition (ALD). Three types of TiO_2 films were deposited: films of un-doped TiO_2 were deposited at 200 and 250 °C, and the films of N-doped TiO_2 were deposited at 250 °C. One sample of each type was left without post-deposition treatment. The rest samples of each type were annealed at temperature ranged from 400 ˚C to 900 °C. Some samples were annealed with nitrogen gas, while others were annealed with oxygen gas. The post-deposited samples exhibited p-type conductivity, which contributed to the presence of oxygen interstitials. Then TiO_2 p-n homojunction diodes were fabricated by a lithography method on silicon wafer as shown in Figure 2(c).

Besides, there are few studies which have been focused on synthesis of intrinsic donor and acceptor defects in TiO_2 simultaneously. Pan *et al.* [20] fabricated TiO_2 p-n homojunction by decorated n-type oxygen-defected TiO_2 on p-type titanium-defected TiO_2. The source of n-type TiO_2 was added to Titanium glycerolate (TiGly) as presented in Figure 2(d). Then the resulting powder of oxygen-defected TiO_2/titanium-defected TiO_2 was calcined in air at 470 °C. Moreover, the titanium vacancies with titanium interstitials could be formed in TiO_2. Wu *et al.* [24] synthesized titanium vacancies-titanium interstitials/TiO_2 by sol gel method with UV light pre-treatment. The titanium vacancies and titanium interstitials were formed when TiO_2 nanoparticles were treated with UV light and its color changed from pale blue to yellow.

4. PROPERTIES OF DEFECTIVE TiO_2 WITH INTRINSIC POINT DEFECTS

4.1 Structural Properties

The intrinsic defects are characterized by different techniques such as X-ray photoelectron spectroscopy (XPS), electron spin resonance (ESR), and Raman spectrometry. Xing *et al.* [38] used solvothermal method with $NaBH_4$ for Ti^{3+}/oxygen vacancies formation in TiO_2. After adding 0.13 g $NaBH_4$ as reduction agent, the samples were washed with HCl. XPS was used to detect the existence of Ti^{3+} ions and oxygen vacancies. As shown in figure 3, after washing the samples with HCl, the peak 458 eV of Ti 2p XPS spectra showed the presence of Ti^{3+} ions. Moreover, peak 531.8 eV on O 1s XPS spectra was related to oxygen vacancies formation.

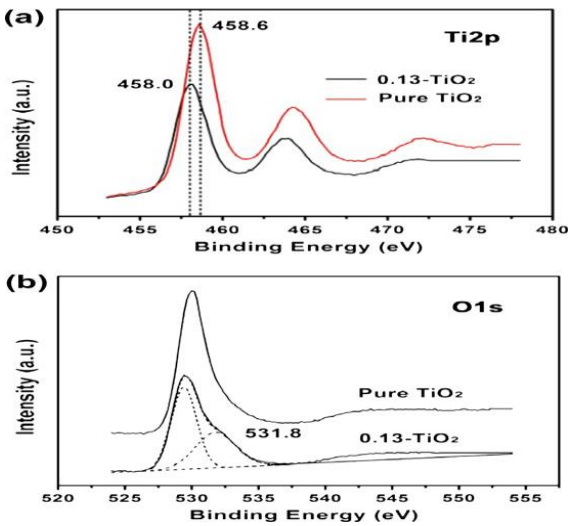

Figure 3. XPS spectra of Ti^{3+} self-doped TiO_2: (a) Ti2p XPS spectra and (b) O1s XPS spectra, the red line of XPS spectra for pure TiO_2 and the black line for reduced TiO_2 with 0.13 g $NaBH_4$ [38].

Ti^{3+} defects which formed in mesoporous black TiO_2/graphene assemblies were investigated by Zhou *et al.* [18]. The XPS spectrum of Ti 2p1/2 and 2p3/2 showed peaks at 463.6 and 457.8 eV which could be assigned to Ti^{4+}. Meanwhile, there were two peaks at 462.7 and 457.0 eV which corresponding to the Ti 2p1/2 and Ti 2p3/2 peaks of Ti^{3+} species. According to O 1s XPs spectrum, the two peaks at 529.8 and 532.1 eV were assigned to Ti-O bond and the -OH group. Yin *et al*. [52] studied the chemical composition of self-doped TiO_2 hierarchical hollow spheres by XPS spectrum. The study observed that after the TiO_2 was reduced by $NaBH_4$, the Ti 2p peak shifted to lower binding energy which could be due to the formation of Ti^{3+} species . The O 1s peak shifted from 529.8 eV to 529.2 eV, which indicated that the electrons transfer from conduction band to oxygen vacancy level. Furthermore, electron paramagnetic resonance (EPR) showed strong signal at 2.002 which could be assigned to oxygen vacancies. Moreover, the super-paramagnetic behavior was observed because of the presence of Ti^{3+} species. As a result, the EPR signal and super-paramagnetic behavior confirmed the existence of oxygen vacancies and Ti^{3+} species in self-doped TiO_2 hierarchical hollow spheres, respectively.

Yang *et al*. [53] analyzed the chemical states of core/shell TiO_2/C nanostructure with Pt loading (TCP) by XPS spectrum. Two peaks at 458.7 (Ti 2p3/2) and 464.5 eV (Ti 2p1/2) were related to Ti^{4+}, while two peaks which were centered at 457.6 and 463.2 eV corresponding to the Ti 2p1/2 and Ti 2p3/2 peaks of Ti^{3+} ions. For O 1s XPS spectra, the peak at 529.2 eV was assigned to Ti^{4+}-O, and the peak at 530.2 eV was assigned to Ti^{3+}-O or -OH. Amano *et al*. [30] calcined TiO_2 with hydrogen gas. Ti^{3+} and oxygen vacancies were characterized by electron spin resonance (ESR) spectra. It was demonstrated that at 500 °C under H_2 treatment signal at g = 2.002 indicated that there were electrons trapped in oxygen vacancies, and at signal g = 1.974 was related to Ti^{3+} species as shown in Figure 4(a). Liu *et al*. [31] synthesized the Ti^{3+} self-doped TiO_2 by high H_2 pressure treatment. The signals (g_{xx} = 1.991, g_{yy} = 1.974 g_{zz} =1.939) of ESR at 4 K, indicated the formation of Ti^{3+} under high H_2 pressure.

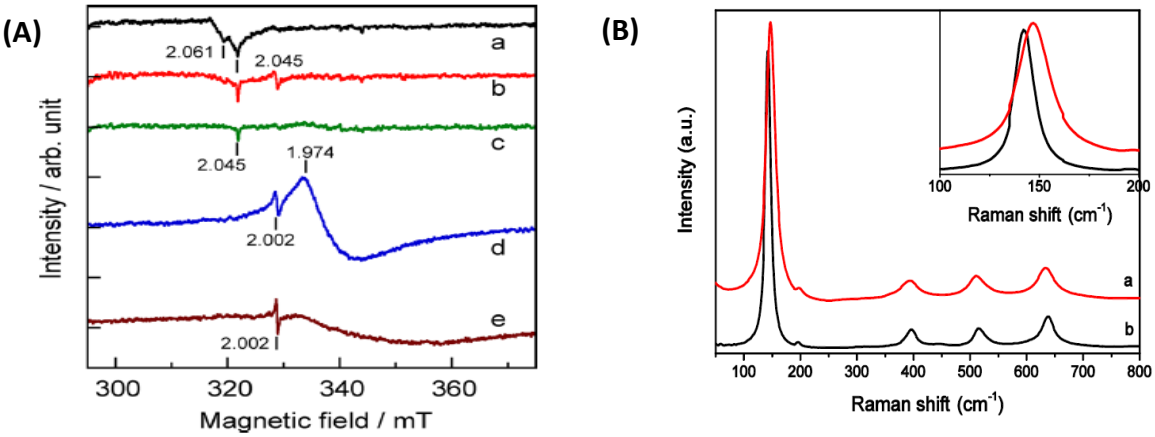

Figure 4. (A) ESR spectra of TiO_2 samples treated: (a) without H_2 treatment, (b) H_2 treatment at 300°C, (c) H_2 treatment at 400°C, (d) H_2 treatment at 500°C, (e) H_2 treatment at 700°C [30]. (B) Raman spectra of: (a) Ti^{3+} self-doped anatase-rutile mixed phase TiO_2, (b) P25-TiO_2 [44].

Xin *et al.* [54] fabricated anatase self-doped TiO_2 nanocrystals by solvothermal method and followed by post-annealing at various temperatures. Raman spectroscopy was employed to investigate the defects in TiO_2. The peak of anatase 144.4 cm^{-1} shifted to 152.6 cm^{-1} and became more broader compared to P25-TiO_2, which indicated the existence of Ti^{3+} with oxygen vacancies or the disorder in the crystal. Zhou *et al.*[44] synthesized Ti^{3+} self-doped anatase-rutile mixed phase TiO_2 using solvothermal method. Raman spectrometry was used to characterize the formation of Ti^{3+}/oxygen vacancies. In comparison to P25-TiO_2, the Raman band at 142 cm^{-1} shifted to 147 cm^{-1} for Ti^{3+} self-doped anatase-rutile mixed phase TiO_2 as is shown in Figure 4(b). The peak shifting of 5 cm^{-1} and broadening ascribed to disorder in TiO_2 which occurred

due to the localized Ti^{3+} associated with oxygen vacancies. Qiu *et al*. [55] used Raman spectrum to detect the presence of Ti^{3+} species in TiO_2 nanocrystal, there were peaks at 146.2 cm^{-1}, 409.1 cm^{-1}, 516.6 cm^{-1}, and 640.1 cm^{-1} due to anatase phase nature. The Eg mode at 144 cm^{-1} and 639 cm^{-1} were shifted to 146.2 cm^{-1} and 640.1 cm^{-1}, respectively, which indicated the formation of Ti^{3+} ions in TiO_2. Wu *et al*. [24] investigated the formation of titanium interstitials and titanium vacancies in the ultra-small yellow TiO_2 nanoparticles. The XPS peak at 456.9 eV which related to Ti^{3+} ions was not found. Moreover, it was observed that the Fermi energy was 1.0 eV which is lower than Fermi level of oxygen vacancies. Thus, the XPS data and Fermi level confirmed the donor intrinsic defects was titanium interstitials. Besides, titanium vacancies were also found. From ESR spectra, the signal g = 1.998 was found due to the formation of titanium vacancies. Wang *et al.* [19] claimed that synthesized TiO_2 by solvothermal method formed titanium vacancies. There was no XPS peaks related to Ti^{3+} or Vo. Furthermore, the ESR signal at g = 1.998 which was not related to Ti^{3+}, Vo, or O^{2-} and was presumably related to titanium vacancies.

4.2 Optical Properties

The intrinsic defects can improve the optical properties of TiO_2. The absorption of sunlight is shifted to the visible or near red-infrared light region duo to the formation of intrinsic point defects energy level between the valence bands and conduction bands of TiO_2 as shown in Figure 5. The calculated energy level are 1.17 eV, 1.23 eV, and 1.15 eV for oxygen vacancies (V_O), titanium interstitials (Ti_{int}), and titanium vacancies (V_{Ti}), respectively [56].

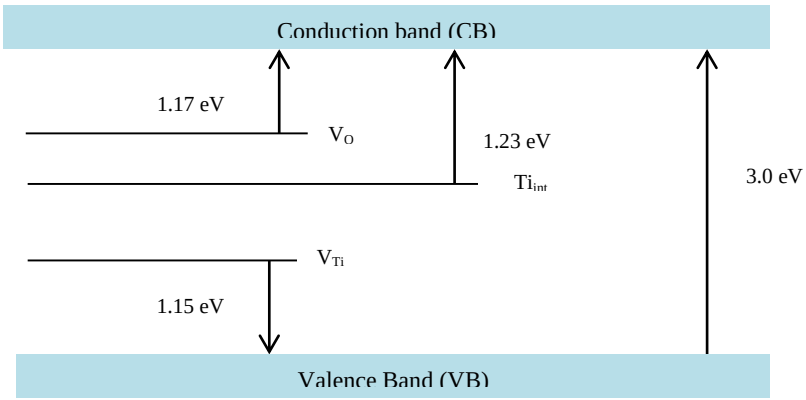

Figure 5. Energy level of oxygen vacancies (V_O), titanium interstitials (Ti_{int}), and titanium vacancies (V_{Ti}) between valence band (VB) and conduction band (CB) of TiO_2, calculated energy level from Ref. [56].

Moreover, due to the formation of energy level of the intrinsic defects, the band gap of TiO_2 is narrowed. Table 2 shows a summary of the narrowed band gap that reported from previous literature. Qui *et al.* [55] synthesized Ti^{3+} self-doped TiO_2 nanocrystals by hydrothermal method based on Le Chatelier's principle. The study investigated the effect of Ti^{3+} and oxygen vacancies on band gap and visible light absorption of TiO_2. The formation method of oxygen vacancies and Ti^{3+} was performed by controlling the ratio between $TiCl_3$ and $(NH_4)_2TiF_6$. It was indicated that the defect of Ti^{3+} and oxygen vacancies prompted the absorption in visible light within the range of 400 nm to 800 nm (Figure 6(a)). The band gap was reduced to 2.68 eV as shown in Figure 6(b). The enhancement of absorption in visible region was due to the reduced band gap of TiO_2. The reduction of the band gap was because of the new mid gap level below conduction band, which produced by Ti^{3+} and oxygen vacancy defects.

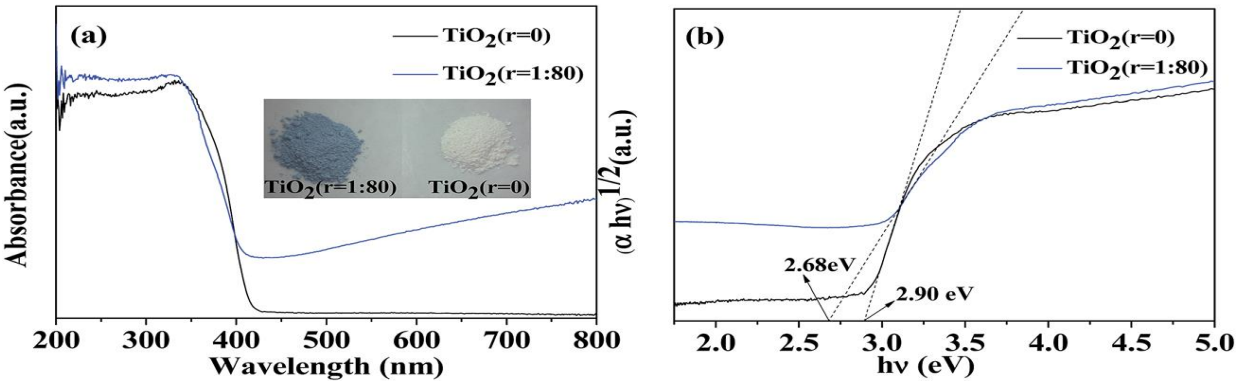

Figure 6. (a) UV-visible diffuse reflectance spectra and (b) band gap of TiO_2 nanocrystals prepared with (r = 1: 80) and without (r = 0) $(NH_4)_2TiF_6$. The inset in (a) shows color-change of the two TiO_2 samples [55].

Xin *et al.* [54] fabricated anatase TiO_2 nanocrystals with different concentration of Ti^{3+} species by solvothermal method and followed by post-annealing. All samples which were treated by post-annealing at different temperatures (300-700°C) showed higher absorption in the longer wavelengths comparison to TiO_{2-x} without post-annealing. The TiO_{2-x} which was annealed at 500 °C had the narrowest band gap (2.63 eV) in comparison to the other samples. The narrowest band gap was ascribed to the abundance of Ti^{3+} in the bulk of TiO_2. Xing *et al.* [38] used $NaBH_4$ as reduction agent for Ti^{3+}-doped TiO_2, and consequently the absorption intensity increased. The Ti^{3+}/TiO_2 with the 0.13 g of $NaBH_4$ showed the highest absorption intensity and the band gap was 2.71 eV. Zhou *et al.* [18] investigated the optical properties of Ti^{3+} self-doped mesoporous black TiO_2/graphene assemblies and mesoporous black TiO_2/graphene assemblies. The existence of Ti^{3+} ions increased the visible light absorption in comparison to mesoporous black TiO_2/graphene assemblies, which exhibited a slight absorption in visible light. Furthermore, the band gap of Ti^{3+} self-doped mesoporous black TiO_2/graphene assemblies was 2.7 eV, while the band gap of mesoporous black TiO_2/graphene assemblies was 3.2 eV. The wide absorption in visible light and narrowed band gap improved the photocatalytic properties due to the synergistic effect of Ti^{3+}, mesoporous TiO_2, and graphene.

Table 2 The band gap of defective TiO_2 with Ti^{3+} and oxygen vacancies.

Started TiO_2	Defect	Band gap (eV)	Reference
TiO_2 nanocrystals	Ti^{3+}, V_O	2.68	[55]
TiO_2 nanocrystals	Ti^{3+}	2.63	[54]
TiO_2 nanoparticles	Ti^{3+}, V_O	2.71	[38]
Mesoporous black TiO_2/graphene assemblies	Ti^{3+}, V_O	2.7	[18]
Ultra-small yellow TiO_2 nanoparticles	Ti_{int}	2.76	[24]

Liu *et al.* [32] fabricated Ti^{3+} self-doped TiO_{2-x} nanoparticles in anatase phase by oxidation of TiH_2 in H_2O_2, then the defective nanoparticles were calcined at different temperatures (300 °C to 600 °C) with various times (2 h to 4 h). It was observed that all samples which were treated at different temperatures and times absorbed the visible light in range between 400 nm and 800 nm and decreased the band gap. It has been demonstrated that although the two samples of TiO_{2-x}, which were treated at 500 °C for 3 h and at 400 °C for 4 h showed strong visible light absorption, these samples also showed weak UV absorption. The strong absorption in visible region ascribed to the untreated TiH_2. Among all samples, TiO_{2-x} at 500 °C for 4 h which had a better crystallinity and higher content of Ti^{3+} exhibited the strongest visible light absorption. Zhou *et al.* [44] prepared Ti^{3+} self-doped anatase-rutile TiO_2 nanoparticles by solvothermal

method. During the samples preparation, the volume ratios of $TiCl_3$ to titanium isopropoxide (0:4, 5:4, 10:4, 15:4, and 30:4) was controlled. When the volume of $TiCl_3$ during synthetic reaction increased, the absorption in visible light increased and optical absorption band edge shifted to longer wavelengths. Furthermore, when the amount of $TiCl_3$ was increased, the band gaps of all samples were decreased. It was noted that the formation of Ti^{3+} defects and the high percentage of rutile phase were associated with decreases in the band gaps of the samples. Similar to Ti^{3+} and oxygen vacancies, titanium interstitials also reduce the band gap and enhance the visible light absorption. The ultra-small yellow TiO_2 nanoparticles with the titanium interstitials/titanium vacancies reduced the band gap to 2.76 eV. This was attributed to the titanium interstitials formation. The sample absorbed the light at 450 nm which related to visible light absorption [24]. However, compared to the intrinsic donor defects, titanium vacancies which as intrinsic acceptor defects do not reduce the band gap of TiO_2. Bak *et al.* [50] synthesized the defective TiO_2 with titanium vacancies by prolong oxidation. The authors evaluated the effect of prolong oxidation on the band gap of TiO_2. It was observed that the wide band gap of TiO_2 was not reduced by prolonged oxidation which formed the titanium vacancies. That means there was no change in band gap before and after the titanium vacancies formation.

4.3 Transfer Charge Properties

In order to obtain an efficient photo-catalyst, the high separation efficiency of photoinduced electron-hole pairs and rapid charge transfer are required. Therefore, numerous studies have focused on the effect of intrinsic defects in TiO_2 on charge separation and transfer. Zhang *et al.* [57] synthesized different types of TiO_2 by hydrothermal; anatase TiO_2 sheet, Ti^{3+} self-doped rutile TiO_2, Ti^{3+} self-doped anatase-rutile TiO_2 sheets (fabricated from anatase TiO_2 sheets), and Ti^{3+} self-doped anatase-rutile mixed phase TiO_2 (fabricated from Degussa P25 TiO_2). The authors investigated the separation efficiency of the photogenerated electron-hole pairs by photoluminescence (PL) spectra. PL intensity of Ti^{3+} self-doped anatase-rutile mixed phase TiO_2 nanosheets was lower than Ti^{3+} self-doped rutile TiO_2. The lower PL intensity indicated much higher charge separation than self-doped rutile due to the transfer of photo-excited charge carriers between anatase and rutile TiO_2 under visible light irradiation. Furthermore, as compared to anatase TiO_2 nanosheets and Ti^{3+}/ rutile TiO_2, self-doped anatase-rutile mixed phase TiO_2 nanosheets showed larger photocurrent. As a result, the PL intensity and photocurrent indicated that Ti^{3+} self-doped anatase-rutile mixed phase TiO_2 nanosheets enhanced significantly the photogeneration charge carriers separations. Amano *et al.* [30] claimed that reduced TiO_2 by hydrogenation at various temperatures showed high donor density and low resistance, which attributed to the increase of n-type conductivity due to increasing amount of conduction electrons. As the electrical conductivity enhanced, the charge carrier recombination reduced and accordingly improve the photocatalytic activity. Deng *et al.* [58] prepared Ti^{3+} self-doped TiO_2 nanorods/nanosheets by hydrothermal method and then treated with $NaBH_4$. The charge carrier transfer and photogenerated electron-hole pairs separation were tested by electrochemical impedance spectroscopy (EIS). The radius on the EIS Nyquist plot of Ti^{3+} self-doped TiO_2 nanorods/nanosheets was smaller than the radius of TiO_2 nanorods/nanosheets both in the dark and under light illumination, which attributed to the enhancement of charge separation and transfer. Thus, the interface resistance became lower and the electrochemical reaction became more facilitated. Xin *et al.* [54] studied the electrochemical properties of Ti^{3+} self-doped anatase TiO_2 nanocrystals (Ti^{3+}/TiO_2 NCs) by EIS. It was observed that the radius of arc in EIS Nyquist plot of Ti^{3+}/TiO_2 NCs was smaller than that samples without Ti^{3+} ions both in the dark and under light irradiation.

Moreover, various studies have investigated the effect of p-type TiO_2 on charge mobility. Table 3 shows the charge mobility of p-type TiO_2 which fabricated and investigated by various studies. Wang e al. [19] conducted a study on the effect of p-type TiO_2 with titanium vacancies on charge mobility and resistivity. The existence of titanium vacancies increased the charge mobility and

decreased the resistivity. Hall Effect measurement was used to determine the type of electrical conductivity and the charge mobility. The Hall coefficient was positive (+134 cm^3/C) for defective TiO_2 with titanium vacancy defects, which indicated the product was p-type and conducted via holes, while n-type TiO_2 exhibited negative Hall coefficient (−33.3 cm^3/C). In addition, the charge mobility of p-type TiO_2 was 1.39×10^{-4} $cm^2/V{\cdot}S$, which was higher than the charge mobility of n-type TiO_2 (0.223×10^{-4} $cm^2/V{\cdot}s$). Furthermore, the Mott–Schottky plots showed negative slope which gave another evidence of the p-type TiO_2 formation. From electrochemical impedance spectra (EIS), the radius in the Nyquist plot of p-type TiO_2 was smaller than the radius of n-type TiO_2, which indicated the titanium vacancies in TiO_2 enhanced the charge transfer between the TiO_2 and the electrolyte interface. As a result, the charge carrier separation increased. Bak ea al. [50] formed titanium vacancies in TiO_2 by prolong oxidation with mixture of argon and oxygen gas. The effect of prolonged oxidation of the TiO_2 on charge mobility was evaluated. The mobility of electrons increased to 0.8×10^{-5} m^2 V^{-1} s^{-1} after 2470 h. Bhowmik *et al.* [51] fabricated p-type TiO_2 by sol–gel method. and then it was deposited on thermally oxidized p-type Si substrate by drop coating. After that the product was annealed in air at 450 °C for 3 h. It was claimed that the charge carrier (hole) concentration and mobility of undoped p-type TiO_2 were 7.893×10^{15} cm^{-3} and 2.198×10^3 cm^2 V^{-1} S^{-1} respectively. Iancu *et al.*[43] synthesized undoped p-type TiO_2 films with oxygen interstitial defects by atomic layer deposition (ALD). The authors observed that the carrier (hole) mobilities of the undoped p-type (with oxygen interstitials) were larger than 400 cm^2 V^{-1} S^{-1}.

Table 3 Charge mobility of p-type TiO_2.

Photocatalyst	Defect	Charge mobility	Reference
P-type TiO_2	V_{Ti}	1.39×10^{-4} $cm^2/V{\cdot}S$	[19]
P-type TiO_2	V_{Ti}	0.8×10^{-5} m^2 V^{-1} s^{-1}	[50]
P-type TiO_2 thin film	O_{int}	2.198 10^3 cm^2 V^{-1} S^{-1}	[51]
P-type TiO_2 thin film	V_{Ti}	400 cm^2 V^{-1} S^{-1}	[43]

5. PHOTOCATALYTIC HYDROGEN PRODUCTION

Hydrogen production by photocatalytic water splitting is measured using two methods: photo-chemical reaction and photo-electrochemical reaction. In photochemical reaction (Figure 7(a)), the powder or thin film photo-catalyst is suspended or immersed in a solution to perform the water splitting reaction. Sacrificial agent is used for photochemical reaction to prevent the charge carrier recombination. Gas chromatograph with thermal conductive detector is used to estimate photocatalytic H_2 evolution rate. On the other hand, in the photoelectrochemical reaction as shown in Figure 7(b), the thin film photocatalyst acts as a working electrode. An external circuit is used to transfer the electrons from the anode to the cathode, where hydrogen is generated. The photoelectrochemical water splitting is evaluated by measuring the photocurrent [59-63].

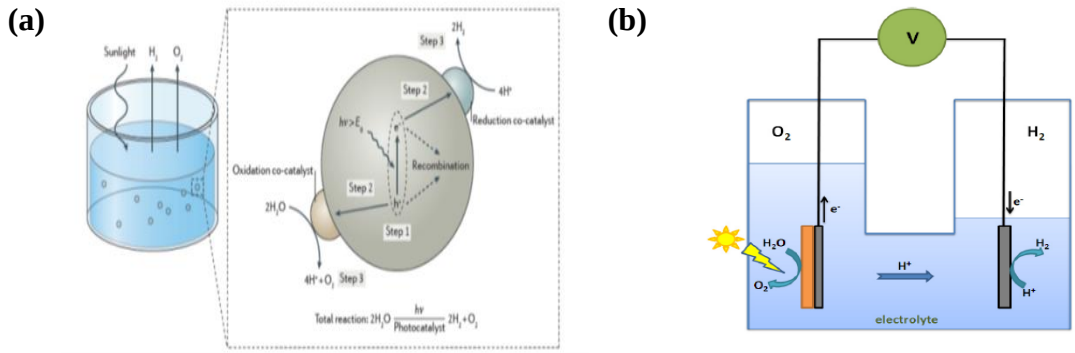

Figure 7. Photocatalytic water-splitting reactions: (a) photo-chemical reaction [62]. (b) photo-electrochemical reaction [59].

In this section, the recent advances of defective TiO_2 with intrinsic point defects for photocatalytic hydrogen evolution and photoelectrochemical water splitting are discussed. Table 4 and Table 5 summarize the photocatalytic hydrogen evolution and photoelectrochemical water splitting of defective TiO_2 with intrinsic point defects, respectively.

5.1 Photocatalytic Hydrogen Evolution

It is essential to measure the photocatalytic activity of TiO_2 for hydrogen evolution in order to know if the modified TiO_2 by different strategies improved the photocatalytic hydrogen generation. Yang *et al.* [53] synthesized core/shell TiO_2/C nanostructure with Pt loading(TCP) to form Ti^{3+} species (Ti^{3+}/TCP). The hydrogen evolution was high (8117 μmol g^{-1} h^{-1}), which ascribed to the absorption of visible light. Furthermore, the carbon layers helped to promote the electrical conductivity which improve the separation and the transfer of photogenerated charge carriers. Most importantly, Ti^{3+}/TCP obtained a good catalytic stability after a 40 h cycle reaction. Tian *et al.[*40] investigated the effect of reduced TiO_2 nanobelts on photocatalytic hydrogen generation. Ti^{3+}/oxygen vacancies was formed in TiO_2 nanobelts by using $NaBH_4$ as a reduction agent. The defects hindered the charge carrier recombination. Furthermore, the defects enhanced the charge carrier trapping and the visible light absorption. Thus, the H_2 evolution of reduced TiO_2 nanobelts (7.02 mmol g^{-1} h^{-1}) was higher than TiO_2 nanobelts (0.67 mmol g^{-1} h^{-1}). Yu *et al.* [64] synthesized Ti^{3+}/TiO_2 mesocrystals which exhibited mesoporous structure. H_2 generation of Ti^{3+}/TiO_2 mesocrystals (301.1 μmol g^{-1} h^{-1}) was higher than P25 TiO_2 (2.3 μmol g^{-1} h^{-1}). The enhanced photocatalytic activity attributed to the formation of Ti^{3+} and mesocrystal structure, resulting in enhancing the visible light absorption and electron-hole pair separation. Wang *et al.* [19] synthesized p-type-TiO_2 with titanium vacancies by solvothermal method. P-type TiO_2 exhibited H_2 evolution of 29.8 mmol g^{-1} h^{-1}, while the normal TiO_2 generated only 6.8 mmol g^{-1} h^{-1}. The existence of the titanium vacancies increased the charge mobility and subsequently the photocatalytic activity also increased. Pan *et al.* [20] investigated the effect of TiO_2 p-n homojunction on photocatalytic hydrogen generation. TiO_2 p-n homojunction showed higher photoactivity for hydrogen evolution than p-type TiO_2 or n-type TiO_2. The hydrogen evolution rate of p-n TiO_2 was 50.3 mmol $h^{-1}g^{-1}$ whereas the hydrogen evolution rate was recorded to be 29.8 mmol $h^{-1}g^{-1}$ and 6.75 mmol g^{-1} h^{-1} for p-type TiO_2 and n-type TiO_2, respectively. Wu *et al.* [24] synthesized TiO_2 with titanium vacancies-titanium interstitials (V_{Ti}-Ti_{int}) by UV light pretreatment. Titanium vacancies-titanium interstitials in TiO_2 enhanced the photocatalytic activity for H_2 generation. Hydrogen evolution was 48.4 μmol g^{-1} h^{-1} under solar simulator illumination. The photocatalysis was enhanced due to V_{Ti}-Ti_{int} formatiom which act as active sites. Li *et al.* [65] created a black Ti^{3+}-doped single-crystal TiO_2 by treated Ti foil in 1-methyl-imidazolium tetrafluoroborate ionic liquid containing acetic acid (HAc), and lithium

acetate (LiAc) under ionothermal conditions. The photocatalytic activity for hydrogen production was 0.26 mmol $h^{-1}m^{-2}$, which was higher than TiO_2 P25 (0.13 mmol $h^{-1}m^{-2}$). The abundance of Ti^{3+} ions in TiO_2 lattice and oxygen vacancies promoted the absorption of visible light and photoelectron-hole separation. Zhao *et al.* [36] produced four types of TiO_2 nanorods: stoichiometric nanorods (TiO_2 NRs), nanorods with surface oxygen vacancies (S-TiO_{2-x} NRs), nanorods with bulk oxygen vacancies (B-TiO_{2-x} NRs), and nanorods with bulk and surface oxygen vacancies (S-B-TiO_{2-x} NRs). S-TiO_{2-x} was treated by $NaBH_4$ reduction, while B-TiO_{2-x} was treated by hydrothermal method. Then, B-TiO_{2-x} was treated by surface reduction treatment with $NaBH_4$ to form S-B-TiO_{2-x} NRs. Under solar-light irradiation, the H_2 evolution rate of S-B-TiO_{2-x} NRs (106.98 μmol/h) was higher than B-TiO_{2-x} NRs (56.58 μmol/h), S-TiO_{2-x} NRs (48.94 μmol/h), and TiO_2 NPs (8.49 μmol/h). All samples of TiO_2 NRs which contain oxygen vacancies showed higher photocatalytic activity in comparison to TiO_2 NRs without the oxygen vacancies. The existence of the oxygen vacancies improved the donor density, photogenerated charge carrier separation, and electronic conductivity.

Hydrothermal method was used to synthesize rice-shaped Ti^{3+} self-doped TiO_{2-x} nanoparticles by oxidation of TiH_2 in H_2O_2. The obtained photocatalyst exhibited higher H_2 evolution rate in comparison to P25 TiO_2 due to the formation of oxygen vacancies and Ti^{3+} ions [66]. Zhou *et al.* [18] formed Ti^{3+} self-doped mesoporous black TiO_2/graphene assemblies by solvothermal method and the product was treated by surface hydrogenation. The two-dimensional graphene structure and TiO_2 mesoporous architecture improved the charge carrier separation and the visible light absorption. Thus, hydrogen evolution rate of Ti^{3+} self-doped mesoporous black TiO_2/graphene assemblies (186 μmol h^{-1} 0.01g^{-1}) was higher than mesoporous black TiO_2/graphene assemblies (~ 50 μmol h^{-1} 0.01 g^{-1}) and mesoporous black TiO_2 (~ 96 μmol h^{-1} 0.01 g^{-1}).

Table 4 Photocatalytic hydrogen evolution of defective TiO_2 with intrinsic point defects

Started TiO_2	Defect	Reactant solution	Light source	H_2 evolution	Reference
TiO_2 nanobelts	Ti^{3+}, V_O	1 wt% Pt & 100 mL aqueous solution containing 20 vol% methanol	350 W Xenon arc lamp (350–750 nm)	7.02 mmol g^{-1} h^{-1}	[40]
Anatase TiO_2	V_{Ti}	1.0 wt. % Pt &120 mL aqueous solution containing 30 vol% methanol	300 W high-pressure Xenon lamp	29.8 mmol g^{-1} h^{-1}	[19]
Anatase TiO_2	V_{Ti} , V_O, Ti^3	1.0 wt. % Pt &120 mL aqueous solution containing 30 vol% methanol	300 W high-pressure Xenon lamp	50.3 mmol g^{-1} h^{-1}	[20]
TiO_2 nanoparticles	V_{Ti}, Ti_{int}	100 ml aqueous solution containing 3.7 vol% formaldehyde	Solar simulator illumination	48.4 μmol g^{-1} h^{-1}	[24]
Black single-crystal TiO_2	Ti^{3+}, V_O	1 wt% Pt & 100 mL aqueous solution with 20 mL methanol	300 W Xenon lamp	0.26 mmol h^{-1} m^{-2}	[65]
TiO_2 nanorods	Ti^{3+}, V_O	1 wt.% Pt & 120 mL aqueous	300 W Xenon lamp	106.98 μmol h^{-1}	[36]

		solution containing 30 vol.% methanol			
TiO_2 nanotube arrays	Ti^{3+}, V_O	methanol/water (50/50 vol %)	AM1.5 (100mW/cm^2)	7 μmol h^{-1} cm^{-2}	[31]
TiO_{2-x} anatase nanoparticles	Ti^{3+}, V_O	0.4 wt% Pt & 150 mL aqueous solution containing 10%, V/V methanol and hexachloroplatinic acid	300 W Xenon lamp	19.9 μmol h^{-1}0.1 g^{-1}	[32]
Black TiO_2	Ti^{3+}, V_O	1 wt% Pt & methanol–water (20%)	Visible light	440 μmol g^{-1} h^{-1}	[67]
TiO_2 nanocrystals	Ti^{3+}	1 wt% & 2 mL aqueous solution containing 50 vol% formic acid	Visible light (> 420 nm, 200 mW cm^{-2})	52 μmol g^{-1} h^{-1}	[68]
Mesoporous black TiO_2	Ti^{3+}	1 wt.% Pt & 80 mL of water and 20 mL of methanol	Solar simulator (equipped with AM 1.5G filter), power density of 100 mW/cm^2	136.2 μmol h^{-1}	[69]
Mesoporous black TiO_2/graphene assemblies	Ti^{3+}, V_O	0.5 wt% & 80 mL of water and 20 mL of methanol	300 W Xenon lamp (equipped with optical cut-off filters)	186 μmol h^{-1} 0.01g^{-1}	[18]
TiO_2	Ti^{3+}, V_O	1% Pt & 120 mL aqueous solution containing 25% methanol	300 W Xenon lamp (equipped with 400nm cut-on filter)	14.8 mmol h^{-1} 0.3 g^{-1}	[48]

5.2 Photoelectrochemical Water Splitting

The improvement in the optical and charge transfer properties have been frequently reported to be responsible for superior Photoelectrochemical performance of defective TiO_2 with intrinsic point defects. There are several studies which evaluated the photoelectrochemical properties of defective TiO_2 by different strategies [70-80]. Deng *et al.* [58] fabricated Ti^{3+} self-doped TiO_2 nanorods/nanosheets photoelectrode by hydrothermal reaction with sodium borohydride reduction. The photocurrent density of the Ti^{3+} self-doped TiO_2 nanorods/nanosheets photoelectrode (0.022 mA cm^{-2}) was higher than the TiO_2 nanorods/nanosheets (0.006 mA cm^{-2}). The Ti^{3+} and oxygen vacancies enhanced the charge carrier separation and the photocatalytic activity. Huo *et al.* [74] synthesized Ti^{3+} self-doped TiO_2 particles by in situ surface hydrogenation synthetic strategy. The photocurrent density of the Ti^{3+}/TiO_2 (1090 nA cm^{-2}) was higher than the TiO_2 (428 nA cm^{-2}). The photoelectrochemical properties of the Ti^{3+}/TiO_2 were improved due to the absorption of visible light. it was found that after switching off the light, the Ti^{3+}/TiO_2 continued to generate current which means the Ti^{3+} extended the lifetimes of charge carrier. In another study, the Ti^{3+} self-doped TiO_2 nanotubes which were fabricated by electrochemical reduction was evaluated for photoelectrochemical activity. The photocurrent of the Ti^{3+} self-doped TiO_2 nanotubes was 0.525 mA cm^{-2}, whereas the photocurrent of the pristine TiO_2 nanotubes was 0.170 mA cm^{-2}. The PEC performance of the Ti^{3+} self-doped TiO_2 nanotubes were improved because the absorbed light was in the visible light region and the charge transfer was accelerated at the TiO_2 and electrolyte interface. Moreover, the Ti^{3+} and oxygen vacancy defects increased the charge density and improved the

electrical conductivity [75]. Lee *et al.* [76] fabricated Ti^{3+} self-doped TiO_2 using sol-gel method and aluminum acetylacetonate was used as catalyst to form Ti^{3+}ions. The enhancement of photo-electrochemical activity correlated to the Ti^{3+} existence. Li *et al.* [77] created Ti^{3+} self-doped TiO_2 nanotube arrays by microwave-assisted chemical reduction method with sodium borohydride. The photocurrent density and photoconversion efficiency under AM1.5 of the Ti^{3+} self-doped TiO_2 nanotube arrays were 3.05 mA cm^{-2} and 1.66% respectively, which were 8 times higher than pristine TiO_2 nanotube arrays. The abundance of Ti^{3+} ion into the bulk of TiO_2 nanotube arrays exhibited stable and enhanced PEC performance as well as efficient absorption of visible light and fast charge carrier separation. One-dimensional Ti^{3+}/ TiO_2 crystals were synthesized by hydrothermal reaction and Ti foil was used as a substrate [78]. The concentration of Ti^{3+} was controlled by N_2H_4 reduction. It was observed that the high level of Ti^{3+} species improved the photoelectrochemical activity, leading to high photocurrent density of 0.64 mAcm^{-2}.

Ti^{3+} self-doped TiO_2 nanoparticles were created by hydrothermal method. Under visible-light irradiation, the obtained photocurrent density of Ti^{3+} self-doped TiO_2 was higher than the photocurrent of pure TiO_2. The existence of Ti^{3+} and oxygen vacancies improved the electrons and holes separation and transportation [24]. Yang *et al.* [79] synthesized Ti^{3+} self-doped TiO_2 nanotube arrays by the electrochemical reduction method. The transient photocurrent density of the Ti^{3+} self-doped TiO_2 nanotube arrays was 3.3 μA cm^{-2}, while the photocurrent of TiO_2 nanotube arrays was 1 μA cm^{-2}. The doping of Ti^{3+} formed shallow donor level separated the photogenerated electron-hole pairs and increased the charge carrier density. As a result, the electrical conductivity improved the charge transfer at semiconductor-electrolyte interface. Furthermore, the light absorption was enhanced by the hierarchical nanotube arrays. In another study, Ti^{3+} self-doped blue TiO_2 single-crystalline nanorods are fabricated by sol-gelation with hydrothermal methods and then reduced by $NaBH_4$. The rod-shape single-crystalline structure and Ti^{3+} with oxygen vacancy formation promoted the charge generation, separation and transfer, leading to higher photocurrent density of 56 μA cm^{-2}, which was 28-fold higher than that of TiO_2 nanoparticles (2 μA cm^{-2}) [17]. Zhang *et al.* [80] prepared Ti^{3+} self-doped black TiO_2 nanotubes with mesoporous nanosheet architecture by solvothermal method. The product was treated by ethylenediamine encircling strategy. The photocurrent of defected TiO_2 was 92.4 μA cm^{-2}, while the photocurrent of non-defected TiO_2 was 51.7 μA cm^{-2}. The enhancement of photoelectrochemical properties was attributed to utilization of wide range of sunlight due to the narrow bandgap. Furthermore, the Ti^{3+} formation improved separation efficiency of the photogenerated charge carriers, and exhibited more surface-active sites.

Table 5 Photoelectrochemical water splitting of defective TiO_2 with intrinsic point defects

Started TiO_2	**Defect**	**Electrolyte**	**Light source**	**Photo-current**	**Reference**
TiO_2 nanorods/nanosheets	Ti^{3+}, Vo	0.1 mol L^{-1} Na_2SO_4	35 W Xenon lamp irradiation	0.022 mA cm^{-2}	[58]
TiO_2 nanoparticles	Ti^{3+}	0.5 mol L^{-1} Na_2SO_4	300 W Xenon lamp	1090 nA cm^{-2}	[74]
TiO_2 nanotubes	Ti^{3+}, Vo	1 M KOH	300 W Xenon arc lamp (equipped with AM 1.5 G filter)	0.525 mA cm^{-2}	[75]
TiO_2 nanoparticles	Ti^{3+}, Vo	0.5 M Na_2SO_4	Simulated solar irradiation, 84.0 mW/cm2	-	[76]
TiO_2 nanotube arrays	Ti^{3+}, V_O	1 M KOH	Simulated solar light (AM1.5, 100 mW cm_2)	3.05 mA cm^{-2}	[77]
One-dimensional TiO_2 crystals	Ti^{3+}	1M KOH	150 W Xenon lamp (equipped with AM 1.5G filter)	0.64 mA cm^{-2}	[78]

TiO_2 nanotube arrays	Ti^{3+}, V_O	1 M KOH	Stimulated sunlight (AM 1.5, 100 mW cm−2)	3.3 μA cm^{-2}	[79]
Blue TiO_2(B) single-crystalline nanorods	Ti^{3+}, V_O	1M KOH	Simulated sunlight AM 1.5	56 μA cm^{-2}	[17]
Black TiO_2 Nanotubes with mesoporous nanosheet architecture	Ti^{3+}, V_O	1 M KOH	AM 1.5 light from a 300 W Xenon lamp	92.4 μA cm^{-2}	[80]
TiO_2 nanotube arrays	Ti^{3+}	1 M KOH	300 W Xenon lamp	2.8 mA cm^{-2}	[70]
TiO_2 nanotubes	Ti^{3+}, V_O	1M KOH	He–Ne laser (632nm)	16.85 mA cm^{-2}	[71]
TiO_2 Nanowire Arrays	V_O	1 M NaOH	150 W Xenon lamp (coupled with an AM 1.5G filter)	1.97 mA cm^{-2}	[72]
Black TiO_2 nanotube arrays	Ti^{3+}, V_O	1 M NaOH	100 mW cm2 illumination	3.65 mA cm^{-2}	[73]
TiO_2 p-n homojunction	Ti^{3+}, V_O, V_{Ti}	0.2 M Na_2SO_4	Xenon lamp (equipped with an AM 1.5G filter)	-1.8 mA cm^{-2}	[20]

6. SUMMARY AND PERSPECTIVE

In this article, we have reviewed recent advances of defective TiO_2 with intrinsic point defects for photocatalytic hydrogen evolution and photoelectrochemical water splitting. The intrinsic point defects in TiO_2 have been developed for solar hydrogen production via solar water splitting. Oxygen vacancy (V_O) and titanium interstitial (Ti_{int}) defects act as intrinsic donor defects, whereas titanium vacancy (V_{Ti}) and oxygen interstitial (O_{int}) defects act as intrinsic acceptor defects. Various preparation methods such as hydrogenation, reduction, oxidation, solvothermal, and atomic layer deposition (ALD) have been utilized to form either intrinsic donor defects or intrinsic acceptor defects. Furthermore, in-situ decoration and UV light assisted sol–gel methods can be used to form the intrinsic donor and acceptor defects simultaneously. Depending on the preparation method and its preparation parameters for formation of intrinsic defects in TiO_2, the structural, optical, charge transfer properties of the TiO_2 can be modified. The defects such as Ti^{3+} and V_O enhance the visible light absorption of solar spectrum due to the narrowing of band gap or formation of midgap states. In addition, the defects improve the photoinduced electron-hole pair separation and significantly promote the charge carrier transfer. Thus, the modified properties enhance the photocatalytic activity for hydrogen production. However, the effect of intrinsic defects on photocatalytic properties for hydrogen production is still far from the satisfactory level. The formation of titanium interstitial (Ti_{int}), titanium vacancy (V_{Ti}), oxygen interstitial (O_{int}), or oxygen vacancy defects in TiO_2 is rarely studied. For future work, the effect of parameters of preparation methods on formation of intrinsic point defects on TiO_2 are needed to be evaluated. The shifting of light absorption from UV to visible region and the adsorption of water molecules on TiO_2 surface for better water splitting should be improved. Moreover, the effect of intrinsic donor and acceptors defects simultaneously on TiO_2 performance for photocatalytic hydrogen generation should be considered. Since TiO_2 is a promising photocatalyst, intrinsic defects would attract more attention for the improvement of TiO_2 performance for photocatalytic hydrogen production.

ACKNOWLEDGEMENTS

This work was financially supported by Contract Grant A043 and U419.

REFERENCES

[1] G. Peharz, F. Dimroth, U. Wittstadt, Solar hydrogen production by water splitting with a conversion efficiency of 18%, Int. J. Hydrogen Energy. **32** (2007) 3248–3252.
[2] B. Wang, S. Shen, S. S. Mao, Black TiO_2 for solar hydrogen conversion, J. Mater. **3** (2017) 96–111.
[3] S. T. Kochuveedu, Photocatalytic and Photoelectrochemical Water Splitting on TiO_2 via Photosensitization, J. Nanomater. 2016 (2016) 1–12.
[4] W. Shangguan, Hydrogen evolution from water splitting on nanocomposite photocatalysts, Sci. Technol. Adv. Mater. **8** (2007) 76–81.
[5] N. L. Panwar, S. C. Kaushik, S. Kothari, Role of renewable energy sources in environmental protection: A review, Renew. Sustain. Energy Rev. **15** (2011) 1513–1524.
[6] T. K. Kim, M. N. Lee, S. H. Lee, Y. C. Park, C. K. Jung, J.-H. Boo, Development of surface coating technology of TiO_2 powder and improvement of photocatalytic activity by surface modification, Thin Solid Films. **475** (2005) 171–177.
[7] L. Y. Ginting, M. K. Agusta, Nugraha, Ahmad H. Lubis, H. K. Dipojono, Cr , Fe – doped anatase TiO_2 photocatalyst : DFT + U Investigation on band gap, Adv. Mater. Res. **893** (2014) 31–34..
[8] R. Jaiswal, N. Patel, D. C. Kothari, A. Miotello, Improved visible light photocatalytic activity of TiO_2 co-doped with Vanadium and Nitrogen, Applied Catal. B, Environ. **126** (2012) 47–54.
[9] F. Dong, S. Guo, H. Wang, X. Li, Z. Wu, Enhancement of the visible light photocatalytic activity of c-doped TiO_2 nanomaterials prepared by a green synthetic approach, J. Phys. Chem. C. **115** (2011) 13285–13292.
[10] R. Jaiswal, J. Bharambe, N. Patel, A. Dashora, D. C. Kothari, A. Miotello, Copper and Nitrogen co-doped TiO_2 photocatalyst with enhanced optical absorption and catalytic activity, "Applied Catal. B, Environ. **168** (2015) 333–341.
[11] E. Albiter, M. A. Valenzuela, S. Alfaro, G. Valverde-Aguilar, F. M. Martínez-Pallares, Photocatalytic deposition of Ag nanoparticles on TiO_2: Metal precursor effect on the structural and photoactivity properties, J. Saudi Chem. Soc. **19** (2015) 563–573.
[12] V. Jovic, W.-T. Chen, D. Sun-Waterhouse, M. G. Blackford, H. Idriss, G. I. N. Waterhouse, Effect of gold loading and TiO_2 support composition on the activity of Au/ TiO_2 photocatalysts for H_2 production from ethanol–water mixtures, J. Catal. **305** (2013) 307–317.
[13] S. Escobedo, B. Serrano, A. Calzada, J. Moreira, H. de Lasa, Hydrogen production using a platinum modified TiO_2 photocatalyst and an organic scavenger. Kinetic modeling, Fuel. **181** (2016) 438–449.
[14] M. C. Wu, I. C. Chang, W. K. Huang, Y. C. Tu, C. P. Hsu, W. F. Su, Correlation between palladium chemical state and photocatalytic performance of TiO_2-Pd based nanoparticles, Thin Solid Films. **570** (2014) 371–375.
[15] H. Wang, L. Zhang, Z. Chen, J. Hu, S. Li, Z. Wang, J. Liu, X. Wang, Semiconductor heterojunction photocatalysts: Design, construction and photocatalytic performances, Chem. Soc. Rev. **43** (2014) 5234–5244.
[16] R. Candal, A. M. la Cruz, New Visible-Light Active Semiconductors, in: Photocatalytic Semicond., Springer International Publishing, Cham, (2015) 41–67.
[17] Y. Zhang, Z. Xing, X. Liu, Z. Li, X. Wu, J. Jiang, M. Li, Q. Zhu, W. Zhou, Ti^{3+} Self-doped Blue TiO_2 (B) single-crystalline nanorods for efficient solar-driven photocatalytic performance, ACS Appl. Mater. Interfaces. **8** (2016) 26851–26859.
[18] G. Zhou, L. Shen, Z. Xing, X. Kou, S. Duan, L. Fan, H. Meng, Q. Xu, X. Zhang, L. Li, M. Zhao, J. Mi, Z. Li, Ti^{3+}self-doped mesoporous black TiO_2/graphene assemblies for unpredicted-high solar-driven photocatalytic hydrogen evolution, J. Colloid Interface Sci. **505** (2017) 1031–1038.

[19] S. Wang, L. Pan, J.-J. Song, W. Mi, J.-J. Zou, L. Wang, X. Zhang, Titanium-defected undoped anatase TiO_2 with p-type conductivity, room-temperature ferromagnetism, and remarkable photocatalytic performance, J. Am. Chem. Soc. **137** (2015) 2975–2983.
[20] L. Pan, S. Wang, J. Xie, L. Wang, X. Zhang, J.-J. Zou, Constructing TiO_2 p-n homojunction for photoelectrochemical and photocatalytic hydrogen generation, Nano Energy. **28** (2016) 296–303.
[21] K. M. Pangan-Okimoto, P. Gorai, A. G. Hollister, E. G. Seebauer, Model for oxygen interstitial injection from the rutile TiO_2 (110) Surface into the Bulk, J. Phys. Chem. C. **119** (2015) 9955–9965.
[22] T. Bak, J. Nowotny, M. K. Nowotny, Defect Disorder of Titanium Dioxide, J. Phys. Chem. B. **110** (2006) 21560–21567.
[23] J. Nowotny, M. A. Alim, T. Bak, M. A. Idris, M. Ionescu, K. Prince, M. Z. Sahdan, K. Sopian, M. A. M. Teridi, W. Sigmund, Defect chemistry and defect engineering of TiO_2-based semiconductors for solar energy conversion, Chem. Soc. Rev. **44** (2015) 8424–8442.
[24] Q. Wu, F. Huang, M. Zhao, J. Xu, J. Zhou, Y. Wang, Ultra-small yellow defective TiO_2 nanoparticles for co-catalyst free photocatalytic hydrogen production, Nano Energy. **24** (2016) 63–71.
[25] L. R. Sheppard, T. Bak, J. Nowotny, Electrical properties of Niobium-doped titanium dioxide. 2. Equilibration Kinetics, J. Phys. Chem. B. **110** (2006) 22455–22461.
[26] M. K. Nowotny, L. R. Sheppard, T. Bak, J. Nowotny, Defect chemistry of titanium dioxide. Application of defect engineering in processing of TiO_2-based photocatalysts, J. Phys. Chem. C. **112** (2008) 5275–5300.
[27] J. Nowotny, T. Bak, M. K. Nowotny, L. R. Sheppard, TiO_2 Surface active sites for water splitting, J. Phys. Chem. B. **110** (2006) 18492–18495.
[28] D. C. Cronemeyer, Infrared absorption of reduced rutile TiO_2 single crystals, Phys. Rev. **113** (1959).
[29] J. Nowotny, A. J. Atanacio, T. Bak, I. V. Belova, S. Fiechter, Y. Ikuma, M. Ionescu, B. J. Kennedy, P. Majewski, G.E. Murch, E.D. Wachsman, Photosensitive oxide semiconductors for solar hydrogen fuel and water disinfection, Int. Mater. Rev. **59** (2014) 449–478.
[30] F. Amano, M. Nakata, A. Yamamoto, T. Tanaka, Effect of Ti^{3+} Ions and conduction band electrons on photocatalytic and photoelectrochemical activity of rutile titania for water oxidation, J. Phys. Chem. C. **120** (2016) 6467–6474.
[31] N. Liu, C. Schneider, D. Freitag, M. Hartmann, U. Venkatesan, J. Müller, E. Spiecker, P. Schmuki, Black TiO_2 Nanotubes: Cocatalyst-Free open-circuit hydrogen generation, Nano Lett. **14** (2014) 3309–3313.
[32] X. Liu, H. Xu, L. R. Grabstanowicz, S. Gao, Z. Lou, W. Wang, B. huang, Y. Dai, T. Xu, Ti^{3+} self-doped TiO_{2-x} anatase nanoparticles via oxidation of TiH_2 in H_2O_2, Catal. Today. **225** (2014) 80–89.
[33] L. R. Grabstanowicz, S. Gao, T. Li, R.M. Rickard, T. Rajh, D.-J. Liu, T. Xu, Facile oxidative conversion of TiH_2 to high-concentration Ti^{3+}-Self-Doped Rutile TiO_2 with Visible-Light Photoactivity, Inorg. Chem. **52** (2013) 3884–3890.
[34] S. Wei, S. Ni, X. Xu, A new approach to inducing Ti^{3+} in anatase TiO_2 for efficient photocatalytic hydrogen production, Chinese J. Catal. **39** (2018) 510–516.
[35] H. Tan, Z. Zhao, M. Niu, C. Mao, D. Cao, D. Cheng, P. Feng, Z. Sun, A facile and versatile method for preparation of colored TiO_2 with enhanced solar-driven photocatalytic activity, Nanoscale. **6** (2014) 10216–10223.
[36] Z. Zhao, X. Zhang, G. Zhang, Z. Liu, D. Qu, X. Miao, P. Feng, Z. Sun, Effect of defects on photocatalytic activity of rutile TiO_2 nanorods, Nano Res. **8** (2015) 4061–4071.
[37] W. Fang, M. Xing, J. Zhang, A new approach to prepare Ti^{3+} self-doped TiO_2 via $NaBH_4$ reduction and hydrochloric acid treatment, Appl. Catal. B Environ. **161** (2014) 240–246.
[38] M. Xing, W. Fang, M. Nasir, Y. Ma, J. Zhang, M. Anpo, Self-doped Ti^{3+}-enhanced TiO_2 nanoparticles with a high-performance photocatalysis, J. Catal. **297** (2013) 236–243.
[39] R. Ren, Z. Wen, S. Cui, Y. Hou, X. Guo, J. Chen, Controllable synthesis and tunable photocatalytic properties of Ti^{3+}-doped TiO_2, Sci. Rep. **5** (2015) 10714.

[40] J. Tian, X. Hu, H. Yang, Y. Zhou, H. Cui, H. Liu, High yield production of reduced TiO_2 with enhanced photocatalytic activity, Appl. Surf. Sci. **360** (2016) 738–743.
[41] Q. Kang, J. Cao, Y. Zhang, L. Liu, H. Xu, J. Ye, Reduced TiO_2 nanotube arrays for photoelectrochemical water splitting, J. Mater. Chem. A. **1** (2013) 5766.
[42] D. Ariyanti, L. Mills, J. Dong, Y. Yao, W. Gao, $NaBH_4$ modified TiO_2: Defect site enhancement related to its photocatalytic activity, Mater. Chem. Phys. **199** (2017) 571–576.
[43] A. T. Iancu, M. Logar, J. Park, F. B. Prinz, Atomic layer deposition of undoped TiO_2 exhibiting p-Type conductivity, ACS Appl. Mater. Interfaces. **7** (2015) 5134–5140.
[44] Y. Zhou, C. Chen, N. Wang, Y. Li, H. Ding, Stable Ti^{3+} Self-Doped anatase-rutile mixed TiO_2 with enhanced visible light utilization and durability, J. Phys. Chem. C. **120** (2016) 6116–6124.
[45] R. Sasikala, V. Sudarsan, C. Sudakar, R. Naik, L. Panicker, S.R. Bharadwaj, Modification of the photocatalytic properties of self doped TiO_2 nanoparticles for hydrogen generation using sunlight type radiation, Int. J. Hydrogen Energy. **34** (2009) 6105–6113.
[46] W. H. Saputera, G. Mul, M. S. Hamdy, Ti^{3+}-containing titania: Synthesis tactics and photocatalytic performance, Catal. Today. **246** (2015) 60–66.
[47] B. Liu, K. Cheng, S. Nie, X. Zhao, H. Yu, J. Yu, A. Fujishima, K. Nakata, Ice–Water quenching induced Ti^{3+} self-doped TiO_2 with surface lattice distortion and the increased photocatalytic activity, J. Phys. Chem. C. **121** (2017) 19836–19848.
[48] F. Zuo, L. Wang, P. Feng, Self-doped Ti^{3+}@ TiO_2 visible light photocatalyst: Influence of synthetic parameters on the H_2 production activity, Int. J. Hydrogen Energy. **39** (2014) 711–717.
[49] M.K. Nowotny, T. Bak, J. Nowotny, C.C. Sorrell, Titanium vacancies in nonstoichiometric TiO_2 single crystal, Phys. Status Solidi. **242** (2005) 88–90.
[50] T. Bak, M. K. Nowotny, L. R. Sheppard, J. Nowotny, Effect of prolonged oxidation on semiconducting properties of titanium dioxide, J. Phys. Chem. C. **112** (2008) 13248–13257.
[51] B. Bhowmik, K. Dutta, A. Hazra, P. Bhattacharyya, Low temperature acetone detection by p-type nano-titania thin film: Equivalent circuit model and sensing mechanism, Solid. State. Electron. **99** (2014) 84–92.
[52] Hy. Yin, Xl. Wang, L. Wang, Ql. N, Ht. Zhao, Self-doped TiO_2 hierarchical hollow spheres with enhanced visible-light photocatalytic activity, J. Alloys Compd. **640** (2015) 68–74.
[53] Y. Yang, P. Gao, X. Ren, L. Sha, P. Yang, J. Zhang, Y. Chen, L. Yang, Massive Ti^{3+} self-doped by the injected electrons from external Pt and the efficient photocatalytic hydrogen production under visible-Light, Appl. Catal. B Environ. **218** (2017) 751–757.
[54] X. Xin, T. Xu, J. Yin, L. Wang, C. Wang, Management on the location and concentration of Ti^{3+} in anatase TiO_2 for defects-induced visible-light photocatalysis, Appl. Catal. B Environ. **176** (2015) 354–362.
[55] M. Qiu, Y. Tian, Z. Chen, Z. Yang, W. Li, K. Wang, L. Wang, K. Wang, W. Zhang, Synthesis of Ti^{3+} self-doped TiO_2 nanocrystals based on Le Chatelier's principle and their application in solar light photocatalysis, RSC Adv. **6** (2016) 74376–74383.
[56] F. M. Hossain, G. E. Murch, L. Sheppard, J. Nowotny, The effect of defect disorder on the electronic structure of rutile TiO_{2-x}, Defect Diffus. Forum. **252** (2006) 1–12.
[57] X. Zhang, G. Zuo, X. Lu, C. Tang, S. Cao, M. Yu, Anatase TiO_2 sheet-assisted synthesis of Ti^{3+} self-doped mixed phase TiO_2 sheet with superior visible-light photocatalytic performance: Roles of anatase TiO_2 sheet, J. Colloid Interface Sci. **490** (2017) 774–782.
[58] X. Deng, H. Zhang, R. Guo, Q. Ma, Y. Cui, X. Cheng, M. Xie, Q. Cheng, Effect of Ti^{3+} on enhancing photocatalytic and photoelectrochemical properties of TiO_2 nanorods/nanosheets photoelectrode, Sep. Purif. Technol. **192** (2018) 329–339.
[59] C. -H. Liao, C. -W. Huang, J. C. S. Wu, Hydrogen production from semiconductor-based photocatalysis via water splitting, Catalysts. **2** (2012) 490–516.

[60] W. -T. Chen, A. Chan, Z. H. N. Al-Azri, A. G. Dosado, M. A. Nadeem, D. Sun-Waterhouse, H. Idriss, G.I.N. Waterhouse, Effect of TiO_2 polymorph and alcohol sacrificial agent on the activity of Au/ TiO_2 photocatalysts for H_2 production in alcohol–water mixtures, J. Catal. **329** (2015) 499–513.
[61] I. S. Cho, Z. Chen, A. J. Forman, D. R. Kim, P. M. Rao, T. F. Jaramillo, X. Zheng, Branched TiO_2 nanorods for photoelectrochemical hydrogen production, Nano Lett. **11** (2011) 4978–4984.
[62] S. Chen, T. Takata, K. Domen, Particulate photocatalysts for overall water splitting, Nat. Rev. Mater. **2** (2017) 17050.
[63] K. Atacan, N. Güy, S. Çakar, Preparation and antibacterial activity of solvothermal synthesized $ZnFe_2O_4$/Ag- TiO_2 nanocomposite, Sak. Univ. J. Sci. **22** (2018) 1720–1726.
[64] X. Yu, X. Fan, L. An, Z. Li, J. Liu, Facile synthesis of Ti^{3+}- TiO_2 mesocrystals for efficient visible-light photocatalysis, J. Phys. Chem. Solids. **119** (2018) 94–99.
[65] G. Li, Z. Lian, X. Liu, Y. Xu, W. Wang, D. Zhang, F. Tian, Ionothermal synthesis of black Ti^{3+}-doped single-crystal TiO_2 as an active photocatalyst for pollutant degradation and H_2 generation, J. Mater. Chem. A. **3** (2015) 3748–3756.
[66] X. Liu, S. Gao, H. Xu, Z. Lou, W. Wang, B. Huang, Y. Dai, Green synthetic approach for Ti^{3+} self-doped TiO_{2-x} nanoparticles with efficient visible light photocatalytic activity, Nanoscale. **5** (2013) 1870–1875.
[67] A. Sinhamahapatra, J. Jeon, J. Yu, A new approach to prepare highly active and stable black titania for visible light-assisted hydrogen production, Energy Environ. Sci. **8** (2015) 3539–3544.
[68] P. Zhang, T. Tachikawa, M. Fujitsuka, T. Majima, Atomic layer deposition-confined nonstoichiometric TiO_2 nanocrystals with tunneling effects for solar driven hydrogen evolution, J. Phys. Chem. Lett. **7** (2016) 1173–1179.
[69] W. Zhou, W. Li, J.Q. Wang, Y. Qu, Y. Yang, Y. Xie, K. Zhang, L. Wang, H. Fu, D. Zhao, Ordered mesoporous black TiO_2 as highly efficient hydrogen evolution photocatalyst, J. Am. Chem. Soc. **136** (2014) 9280–9283.
[70] Z. Zhang, M.N. Hedhili, H. Zhu, P. Wang, Electrochemical reduction induced self-doping of Ti^{3+} for efficient water splitting performance on TiO_2 based photoelectrodes, Phys. Chem. Chem. Phys. **15** (2013) 15637–15644.
[71] L. Aïnouche, L. Hamadou, A. Kadri, N. Benbrahim, D. Bradai, Solar Energy Materials & Solar Cells Ti^{3+} states induced band gap reduction and enhanced visible light absorption of TiO_2 nanotube arrays : Effect of the surface solid fraction factor, Sol. Energy Mater. Sol. Cells. **151** (2016) 179–190.
[72] G. Wang, H. Wang, Y. Ling, Y. Tang, X. Yang, R.C. Fitzmorris, C. Wang, J.Z. Zhang, Y. Li, Hydrogen-treated TiO_2 nanowire arrays for photoelectrochemical water splitting, Nano Lett. **11** (2011) 3026–3033.
[73] H. Cui, W. Zhao, C. Yang, H. Yin, T. Lin, Y. Shan, Y. Xie, H. Gu, F. Huang, Black TiO_2 nanotube arrays for high-efficiency photoelectrochemical water-splitting, J. Mater. Chem. A. **2** (2014) 8612–8616.
[74] J. Huo, Y. Hu, H. Jiang, C. Li, In situ surface hydrogenation synthesis of Ti^{3+} self-doped TiO_2 with enhanced visible light photoactivity, Nanoscale. **6** (2014) 9078–9084.
[75] J. Song, M. Zheng, X. Yuan, Q. Li, F. Wang, L. Ma, Y. You, S. Liu, P. Liu, D. Jiang, L. Ma, W. Shen, Electrochemically induced Ti^{3+} self-doping of TiO_2 nanotube arrays for improved photoelectrochemical water splitting, J. Mater. Sci. **52** (2017) 6976–6986.
[76] J. Lee, Z. Li, L. Zhu, S. Xie, X. Cui, Ti^{3+} Self-Doped TiO_2 via facile catalytic reduction over Al $(acac)_3$ with enhanced photoelectrochemical and photocatalytic activities, "Applied Catal. B, Environ. **224** (2018) 715–724.
[77] H. Li, J. Chen, Z. Xia, J. Xing, Microwave-assisted preparation of self-doped TiO_2 nanotube arrays for enhanced photoelectrochemical water splitting, J. Mater. Chem. A. **3** (2015) 699–705.

[78] C. Mao, F. Zuo, Y. Hou, X. Bu, P. Feng, In situ preparation of a Ti^{3+} self-doped TiO_2 film with enhanced activity as photoanode by N2 H4 Reduction, Angew. Chemie. **126** (2014) 10653–10657.
[79] Y. Yang, J. Liao, Y. Li, X. Cao, N. Li, C. Wang, S. Lin, Electrochemically self-doped hierarchical TiO_2 nanotube arrays for enhanced visible-light photoelectrochemical performance: an experimental and computational study, RSC Adv. **6** (2016) 46871–46878.
[80] X. Zhang, W. Hu, K. Zhang, J. Wang, B. Sun, H. Li, P. Qiao, L. Wang, W. Zhou, Ti^{3+} Self-doped black TiO_2 nanotubes with mesoporous nanosheet architecture as efficient solar-driven hydrogen evolution photocatalysts, ACS Sustain. Chem. Eng. **5** (2017) 6894–6901.